

# Steady MHD Williamson Nanofluid Flow Past an Inclined Stretching Sheet in the Presence of Heat Generation, Chemical Reaction and Aligned Magnetic Field

George Buzuzi, Mangwiro Magodora, Martin T Kudinha,  
William M Manamela, Mobele H Mambo

**Abstract**—Numerical investigation on the influence of effective Prandtl number on the steady MHD Williamson nanofluid flow over an inclined stretching surface in the presence of aligned magnetic field, heat generation and chemical reaction is carried out. By applying a suitable similarity transformation, the system of non-linear coupled partial differential equations are converted to a system of non-linear coupled ordinary differential equations. Numerical solutions of these equations are obtained by using MATLAB package, bvp4c. The impact of various parameters on the velocity, temperature and nanoparticle volume fraction, skin friction, Nusselt number and Sherwood number are discussed through the aid of graphs and tabulated data. The numerical computations reveal that the escalating values of the effective Prandtl number suppresses the concentration profile closer to the wall, the temperature profile and the velocity profile. Furthermore, the velocity is largest when both the channel slope and the magnetic field inclination angles are lowest. The inclination angles have opposite effect on the temperature and concentration profiles. Moreover, results show that varying the Eckert number and the magnetic parameter will have no effect on the skin friction coefficient, Nusselt number and Sherwood number whenever the Brownian motion parameter and the thermophoresis parameter have the same value.

**Index Terms** – Williamson nanofluid, MHD, aligned magnetic field, inclined stretching surface, effective Prandtl number.

## I. INTRODUCTION

Numerous authors have gained interest in the study of non-Newtonian MHD fluid flow. The current study examines the effect of effective Prandtl number on MHD Williamson nanofluid over an inclined sheet, with aligned magnetic field, heat generation and chemical reaction.

Manuscript received May 26, 2023; revised February 16, 2024;

George Buzuzi is a mathematics senior lecturer at the Department of Mathematics and Physics, Cape Peninsula University of Technology, P O Box 1906, Belville, 7535, South Africa (email: buzuzig@cput.ac.za).

Mangwiro Magodora is a mathematics lecturer and current head of the Statistics and Mathematics Department, Bindura University of Science Education, P Bag 1020, Bindura, Zimbabwe, (corresponding author phone: +263 77 432 4963; email: mmagodora@buse.ac.zw.)

Martin Kudinha is a physics lecturer at the Department of Mathematics and Physics, Cape Peninsula University of Technology, P O Box 1906, Belville, 7535, South Africa (email: kudinham@cput.ac.za).

William Malose Manamela is a mathematics lecturer at the Department of Mathematics and Physics, Cape Peninsula University of Technology, P O Box 1906, Belville, 7535, South Africa (email: manamelawi@cput.ac.za).

Mobele H Mambo is a mathematics lecturer at the Department of Mathematics and Physics, Cape Peninsula University of Technology, P O Box 1906, Belville, 7535, South Africa (email: mamboh@cput.ac.za).

Williamson fluid, which is non-Newtonian, exhibits viscous and elastic properties. Fluids which are non-Newtonian, viscous and elastic are also known as pseudo-plastic fluids. In 1929, Williamson [29] discovered the Williamson model. Bilal *et al.* [2] investigated heat transfer and temperature dependency of a 3 dimensional Williamson fluid past a non-linear stretching surface. Lyubimova *et al.* [11] examined the stability of quasi-equilibrium states of a Williamson fluid in an environment of zero gravity. On the other hand, Subbarayudu *et al.* [28] examined time-dependence of radiative Williamson fluid flow against some block.

Choi [6] was the first to discover nanofluids which have transformed the field of fluid dynamics. Nanofluids consist of a mixture of a base fluid and nano-particles (1-100nm) which are known to enhance the fluid thermal conductivity (Khan *et al.* [8], Hunegnaw [7]). While early studies on nanofluids focused on Newtonian fluid, recent studies have established that the fluid rheological properties of nanofluids can be successfully studied using a non-Newtonian model hence most recent studies have focused on non-Newtonian fluids. Nadeem and Hussain [12] studied Williamson nanofluid heat transfer. Krishnamurthy [10] investigated the impact of heat transfer and chemical reaction of steady MHD Williamson nanofluid in a porous medium. MHD heat transfer of Williamson nanofluids subjected to varying thickness and thermal conductivity over a stretching sheet was presented by Reddy *et al.* [13]. Khan *et al.* [8] investigated the effect of inclined Lorentz force on MHD Williamson nanofluid past a non-linear stretching sheet. The examination of MHD nonofluids flow with heat and mass transfer over a stretching sheet through a porous medium was done by Shawky *et al.* [27]. Furthermore, Wubshet and Mekonnen [30] studied the effect of activation energy on MHD Williamson nanofluid flow over a stretching cylinder. Hunegnaw [7] analyzed the unsteady MHD Williamson nanofluid flow over a heated permeable stretching sheet embedded in a porous medium. In the same year, Bouslimi *et al.* [3] investigated the effects of joule heating, thermal radiation, heat generation and chemical reaction on MHD Williamson nanofluid flow over a stretching sheet.

The flow of fluid past inclined surface has caught the attention of a number of researchers. The detailed study of flow along inclined plane has been given by many investigators who among them are [Alam *et al.* [1], Buzuzi and Buzuzi [4], Buzuzi [5], Gurran *et al.* [15], Jain and Kumari [16], Rafique *et al.* [23]]. With regard to Williamson flow, Rafique and

Alotaibi investigated the numerical simulation of Williamson nanofluid flow over an inclined surface. In all the studies carried out it has been found that the effect of increasing the angle of inclination of the flow surface is to reduce the velocity profile and enhance temperature profile and the skin friction.

Investigations on the effect of the aligned magnetic field on MHD fluid flow have received attention of some authors lately. Studies on aligned magnetic field on MHD flow were carried out by authors who among them are, Buzuzi [5], Gopel *et al.* [14] and Sandeep and Sugunamma [26]. Nadeem and Akram [21] examined the influence of inclined magnetic field on peristaltic flow of a Williamson fluid model in an inclined symmetric or asymmetric channel. Studies have revealed that the impact of enhancing the inclination angle of the magnetic field is to strengthens the magnetic field and to decrease the velocity profile of the flow.

Thermal radiation involves heat transfer whereby heat is transferred through the fluid particles. The transfer of heat finds application in the polymer industry, nuclear engineering, design of turbines, and propulsion devices for aircraft missiles. The knowledge of radiation heat transfer in a given system helps in the control of the characteristics or attributes of the final product. Numerous researchers have investigated the effect of thermal radiation under varying conditions. The researchers who studied thermal radiation include among others, Ibrahim *et al.* [18], Roja *et al.* [25], Seddeek and Muguid [31] and Buzuzi [5]. Studies carried out by Mgyari [19], Magyari and Pantokratoras [20] and Buzuzi [5] have shown that for linearized Rosseland approximation, the effect of the radiation parameter and the Prandtl number on the flow should not be studied separately since the effect of one differs with the other in magnitude only and thus a more realistic approach would be to consider the combined effect of both the Prandtl number and the radiation parameter, called the effective Prandtl number. For this reason, our current investigation, considers the impact of the effective Prandtl number rather than the effect of the radiation parameter  $R$  and Prandtl number  $P_r$  separately.

In most of the studies mentioned, researchers investigated fluid flow involving either aligned magnetic field or inclined flow surface but not both. Recently however, a few authors have analysed the effect of both aligned magnetic field and inclined flow surface. Nadeem and Akram [21], Reddy *et al.* [24], Sivaraj and Sheremet [33], Buzuzi [5] and Kumar *et al.* [17] are among the few authors who examined the impact of both aligned magnetic field and inclined flow surface. Although most of these authors discussed the effect of the inclination angles separately, Buzuzi [5], studied the combined effect of both aligned magnetic field and inclined surface on MHD free convective newtonian flow. The present study attempts to address the combined effect of the inclination angles on Williamson nanofluid flow in contrast to Buzuzi [5] who investigated the effect of the inclination angles on Newtonian flow. Furthermore, the current studies differs from that of Nadeem and Akram [21] in that the inclination angles were considered separately and the influence of the effective Prandtl number, heat generation, and other parameters were not considered.

As far as we know, no investigation has been conducted which analyzes the effective Prandtl number effect on MHD Williamson nanofluid flow over an inclined stretching sheet with variable magnetic field, chemical reaction and heat generation and hence the study was carried out to fill the literature gap.

Section 2 of the report discusses the basic equations, particularly their formulation. This is followed by Section 3 which dwells on the solution approach. The findings of the research and their discussion is dealt with in Section 4. Finally, the concluding remarks are presented in Section 5.

## II. MATHEMATICAL DESCRIPTION

Consider a steady 2-dimensional MHD Williamson nanofluid past an inclined stretching surface. The surface is stretching with velocity  $U_w = c_1x$  where  $c_1 > 0$  is a stretching parameter. The flow configuration and coordinate system are shown in Figure 1 with the  $x$ -axis directed along the stretching sheet in the direction of the sheet motion and the  $y$ -axis normal to it. The stretching surface is inclined at an angle  $\gamma$  from the vertical. A magnetic field of uniform strength  $B_0$  is applied at an angle  $\vartheta$  with the  $x$ -axis. The

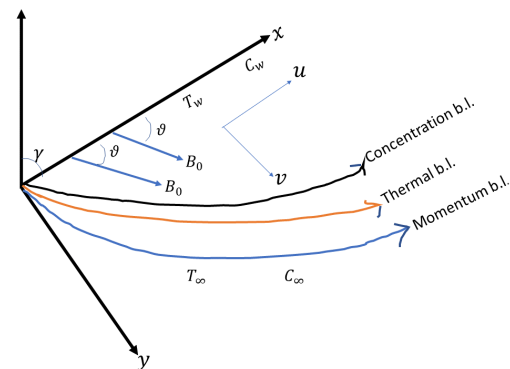


Figure 1: Flow geometry

velocity, temperature and nanofluid concentration of the fluid within the surface vicinity are denoted by  $U_w, T_w, C_w$  respectively. The temperature and concentration further away from the surface are denoted by  $T_\infty$  and  $C_\infty$  respectively. Related to the current Williamson flow model, the Cauchy stress  $S$  is defined as [21]:

$$S = -pI + \tau \tag{1}$$

where the extra stress tensor  $\tau$  is given by

$$\tau = \left[ \mu_\infty + \frac{(\mu_0 - \mu_\infty)}{1 - \gamma^*} \right] A_1, \tag{2}$$

where  $\mu_0$  is the limiting viscosity at zero shear rate,  $\mu_\infty$  is the limiting viscosity at the infinite shear rate,  $\Gamma > 0$  is the time constant and  $A_1$  signifies Rivlin-Ericksen tensor. If we consider the case  $\mu_\infty$  and  $\Gamma\gamma < 1$ , the extra stress tensor reduces to

$$\tau = \mu_0[1 + \Gamma\gamma^*]A_1. \tag{3}$$

According to the above assumptions, the 2-dimensional boundary layer equations governing the flow are given by

[10]:

$$u \frac{\partial u}{\partial x} + v \frac{\partial u}{\partial y} = \nu \frac{\partial^2 u}{\partial y^2} - \sqrt{2\nu}\Gamma \frac{\partial u}{\partial y} \frac{\partial^2 u}{\partial y^2} \quad (4)$$

$$+ \frac{\sigma B_0^2 \sin^2 \vartheta_1}{\rho} - \frac{\nu}{K} u$$

$$+ g\beta_r(T - T_\infty) \cos \gamma_1 + g\beta_m(C - C_\infty) \cos \gamma_1$$

$$u \frac{\partial T}{\partial x} + v \frac{\partial T}{\partial y} = \alpha \frac{\partial^2 T}{\partial y^2} \quad (5)$$

$$+ \tau \left[ D_B \frac{\partial C}{\partial y} \frac{\partial T}{\partial y} + \frac{D_T}{T_\infty} \left( \frac{\partial T}{\partial y} \right)^2 \right] + \frac{Q_0(T - T_\infty)}{(\rho c_p)_f}$$

$$- \frac{1}{(\rho c_p)_f} \frac{\partial q_r}{\partial y} + \frac{(\sigma B_0^2 \sin^2 \vartheta_1) u^2}{(\rho c_p)_f}$$

$$u \frac{\partial C}{\partial x} + v \frac{\partial C}{\partial y} = D_B \frac{\partial^2 C}{\partial y^2} + \frac{D_T}{T_\infty} \frac{\partial^2 T}{\partial y^2} - K_{rp}^*(C - C_\infty) \quad (6)$$

where  $u$  and  $v$  are the components of dimensional velocities along the  $x$  and  $y$  directions respectively.  $T$  is the fluid temperature and  $C$  is the fluid concentration.  $g$  is the gravitational acceleration,  $\nu$  is the kinematic viscosity,  $\alpha$  is the thermal diffusivity,  $\beta_r$  is the coefficient of thermal expansion,  $\beta_m$  is the volumetric coefficient of expansion with concentration,  $B_0$  is the constant magnetic field intensity,  $D_B$  is the Brownian diffusion coefficient,  $D_T$  is the thermophoretic diffusion coefficient,  $\kappa$  is the thermal conductivity of the fluid,  $T_\infty$  is the ambient fluid temperature,  $Q_0$  is the volumetric heat generation,  $K_{rp}^*$  is the chemical reaction parameter,  $K$  is the permeability parameter,  $c_p$  is the specific heat at constant pressure,  $\sigma$  is the electrical conductivity,  $\rho$  is the density of the nanofluid and  $(\rho c_p)_f$  is the heat capacity of the fluid.

The boundary conditions are

$$u = U_w(x) = d_1 x, v = 0, T = T_w, C = C_w \text{ at } y = 0,$$

$$u \rightarrow 0, T \rightarrow T_\infty, C \rightarrow C_\infty \text{ as } y \rightarrow \infty \quad (7)$$

The radiant heat flux  $q_r$  is described using Rosseland approximation as

$$q_r = -\frac{4\sigma^*}{3K^*} \frac{\partial T^4}{\partial y} \quad (8)$$

where  $\sigma^*$  is the Stefan-Boltzman constant,  $K^*$  is the mean absorption coefficient. Following Shateyi *et al.* [32] the difference in temperature within the flow are such that  $T^4$  can be expressed as a linear combination of the temperatures.  $T^4$  is expanded in Taylor series about  $T_\infty$  and higher order terms beyond the first degree are truncated to give

$$T^4 \approx -3T_\infty^4 + 4T_\infty^3 T \quad (9)$$

Therefore

$$q_r = \frac{-16\sigma^* T_\infty^3}{3K^*} \frac{\partial T}{\partial y}$$

$$u \frac{\partial T}{\partial x} + v \frac{\partial T}{\partial y} = \alpha \frac{\partial^2 T}{\partial y^2} \quad (10)$$

$$+ \tau \left[ D_B \frac{\partial C}{\partial y} \frac{\partial T}{\partial y} + \frac{D_T}{T_\infty} \left( \frac{\partial T}{\partial y} \right)^2 \right] + \frac{Q_0(T - T_\infty)}{(\rho c_p)_f}$$

$$+ \frac{1}{(\rho c_p)_f} \frac{16\sigma^* T_\infty^3}{3K^*} \frac{\partial^2 T}{\partial y^2} + \frac{(\sigma B_0^2 \sin^2 \vartheta_1) u^2}{(\rho c_p)_f}$$

We introduce the following similarity transformations in the equations (4) - (6) and boundary conditions (7):

$$u = d_1 x f'(\eta), v = -\sqrt{d_1 \nu} f(\eta),$$

$$\eta = \left( \frac{d_1}{\nu} \right)^{1/2} y, T - T_\infty = (T_w - T_\infty) \theta(\eta), \quad (11)$$

$$C - C_\infty = (C_w - C_\infty) \phi(\eta),$$

where  $f(\eta)$ ,  $\theta(\eta)$ ,  $\phi(\eta)$ , are the dimensional stream function, temperature distribution function, concentration distribution functions, respectively. By substituting (11) into (4)- (6) we get the following non-dimensional, non-linear and coupled ordinary differential equations:

$$f''' + f f'' - (f')^2 + W_p f'' f''' + G_t \theta \cos \gamma_1$$

$$+ G_m \phi \cos \gamma_1 - D_c f' - M_p f' \sin^2 \vartheta_1 = 0 \quad (12)$$

$$\theta'' + E_{f_{pn}} [f \theta' + N_b \phi' \theta' + N_t (\theta')^2 + H_g \theta]$$

$$+ E_{f_{pn}} M_p E_c f'^2 \sin^2 \vartheta_1 = 0 \quad (13)$$

$$\phi'' + N_{tb} \theta'' - K_{rp} Le \phi + Le f \phi' = 0 \quad (14)$$

The associated boundary conditions are:

$$f'(\eta) = 1, \theta(\eta) = 1, \phi(\eta) = 1 \text{ at } \eta = 0,$$

$$f'(\eta) = 0, \theta(\eta) = 0, \phi(\eta) = 0, \text{ as } \eta \rightarrow \infty, \quad (15)$$

where the prime denote differentiation with respect to  $\eta$  where  $E_{f_{pn}} = 3P_r/(3 + 4R_d)$  is the effective Prandtl number,  $P_r = \nu/\alpha$  is the the Prandtl number,  $R_d = 4\rho T_\infty^3/\kappa K$  is the radiation parameter,  $W_p = \Gamma x \sqrt{2d_1^3/\nu}$  is the non-Newtonian Williamson parameter,  $D_c = \nu/Kd_1$  is the Darcy number,  $H_g = Q_0/\rho d_1 c_p$  is the heat generation parameter,  $G_r = g\beta_r(T_w - T_\infty)/d_1^2 x$  is the local thermal Grashof number,  $G_m = g\beta_m(C_w - C_\infty)/d_1^2 x$  is the local solutal Grashof number,  $M_p = \sigma B_0^2/\rho d_1$  is the magnetic field parameter,  $Le = \nu/D_B$  is the Lewis number,  $E_c = U_w^2/c_p(T_w - T_\infty)$  is the Eckert number,  $N_t = \tau D_T(T_w - T_\infty)/\nu T_\infty$  is the thermophoresis parameter,  $N_b = \tau D_B(c_w - c_\infty)/\nu$  is the Brownian motion parameter,  $N_{tb} = N_t/N_b$  and  $K_{rp} = K_{rp}^*/d_1$  is the chemical reaction parameter.

Physical quantities which are impactful from the engineering point of view are the local skin friction coefficient  $C_f$ , the local Nusselt number  $Nu_x$  and the local Sherwood number  $Sh_x$ .

The skin friction, Nusselt number and Sherwood number are, respectively expressed as

$$C_f = \tau_w / \rho U_w^2, Nu_x = xq_w^* / k(T_w - T_\infty) \text{ and } Sh_x = xq_m^* / D_B(C_w - C_\infty)$$

where

$$q_w^* = -k \left[ \frac{\partial T}{\partial y} \right]_{y=0}, q_m^* = D_B \left[ \frac{\partial C}{\partial y} \right]_{y=0}, \tau_w = \mu \left[ \frac{\partial u}{\partial y} + \frac{\Gamma}{\sqrt{2}} \left( \frac{\partial u}{\partial y} \right)^2 \right]_{y=0}$$

The related expressions of the dimensionless variables are

$$Re_x^{1/2} C_f = [1 + 0.5W_p f''(0)] f''(0), Re_x^{-1/2} Nu_x = -\theta'(0),$$

$$Re_x^{-1/2} Sh_x = -\phi'(0). \tag{16}$$

where  $Re_x = \frac{d_1 x^2}{\nu}$  is the local Reynolds number.

### III. SOLUTION APPROACH

The coupled ordinary differential equations (12)-(14) together with associated boundary conditions (15) solved using MATLAB **bvp4c** package. Let

$$\frac{df}{d\eta} = y_2,$$

$$\frac{d^2 f}{d\eta^2} = y_3,$$

$$\frac{d^3 f}{d\eta^3} = \frac{1}{1 + W_p y_3} [y_2^2 + D_c y_2 + M_p y_2 \sin^2 \vartheta_1 - y_1 y_3$$

$$-G_r y_4 \cos \gamma_1 - G_m y_6 \cos \gamma_1,$$

$$\frac{d\theta}{d\eta} = y_5$$

$$y_5' = -E_{fpm} [y_1 y_5 + N_b y_7 y_5 + N_t y_5^2 + H_g y_4 + M_p E_c y_2^2 \sin \vartheta_1]$$

$$\frac{d\phi}{d\eta} = y_7,$$

$$y_7' = K_{rp} L_e y_6 - L_e y_1 y_7$$

$$+ N_{tb} E_{fpm} [y_1 y_5 + N_b y_7 y_5 + N_t y_5^2 + H_g y_4 + M_p E_c y_2^2 \sin^2 \vartheta_1] \tag{17}$$

with the accompanying boundary conditions:

$$y_2(0) = 1, y_4(0) = 1, y_6(0) = 1, y_2(10) = 0, y_4(10) = 0, y_6(10) = 0, \tag{18}$$

The value  $\eta_{max} = 10$  was considered the best choice since all the asymptotic numerical solutions approached the  $\eta_{max}$  value appropriately.

### IV. RESULTS AND DISCUSSION

Numerical simulations of Williamson nanofluid over inclined flow surface subjected to aligned magnetic field are presented. The role of the relevant flow variables such as the effective Prandtl number

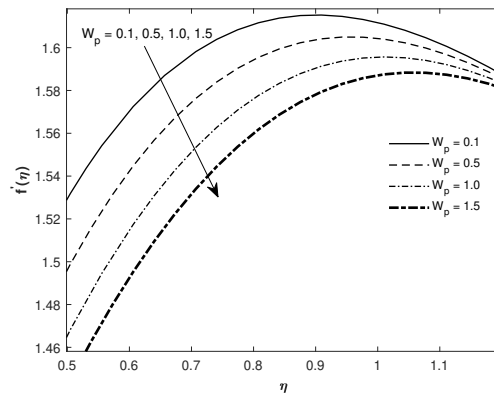


Figure 2: Velocity variation for varying values of  $W_p$  with  $E_{fpm} = 0.01, M_p = 1, \vartheta = 90, \gamma = 0, G_t = 5, L_e = 0.3, G_m = 1, N_t = N_b = 0.1$

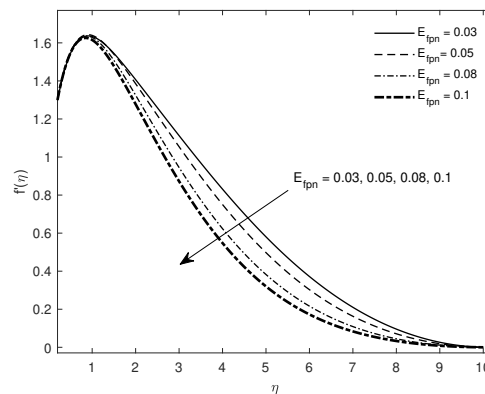


Figure 3: Velocity variation for varying values of  $E_{fpm}$  with  $W_p = 0.3, K_{rp} = 0.1, M_p = 1, H_g = 0.4, \vartheta = 90, \gamma = 0, L_e = 0.3, G_t = 5, G_m = 1, N_t = N_b = 0.1$ .

$E_{fpm}$ , thermophoresis parameter  $N_t$ , Brownian motion parameter  $N_b$ , heat generation parameter  $H_g$ , magnetic parameter  $M_p$ , non-Newtonian Williamson factor  $W_p$ , Darcy number  $D_c$ , Lewis number  $L_e$ , local Grashof number  $G_t$ , modified Grashof number  $G_m$ , aligned magnetic field parameter  $\vartheta_1$ , and channel inclination parameter  $\gamma_1$  on the velocity, temperature, concentration, skin friction coefficient, heat transfer rate and mass transfer rate are investigated. Table I portrays a comparison of the present result with existing results by Khan and Pop [9] and Rafique and Alotaibi [22]. The excellent agreement among the compared results confirms the accuracy of the current numerical algorithm used.

Table I: The Nusselt number values for various values of  $N_t$  and  $N_b$  with  $Pr = Le = 10, M_p = G_t = G_m = K_{rp} = W_p = H_g = K_{rp} = 0, \gamma_1 = 90, D_c = 1$ .

		Khan[9]	Rafique[22]	Present Results
$N_b$	$N_t$	$-\theta'(0)$	$-\theta'(0)$	$-\theta'(0)$ height0.1
0.1	0.9524	0.9524	0.9524	
0.3	0.3	0.1355	0.1355	0.1355
0.5	0.5	0.0179	0.0179	0.0179

The impact of the stretching sheet inclination  $\vartheta_1$  and the magnetic field inclination  $\gamma_1$  on the velocity distribution, temperature distribution and nanoparticle volume fraction is described in Figures 7, 14 and 23, respectively. It is shown on Figure 7 that larger values of  $\vartheta_1$  and  $\gamma_1$  diminish the velocity field. Also, the magnitude of the velocity profile is greatest when both the inclination angles are lowest,

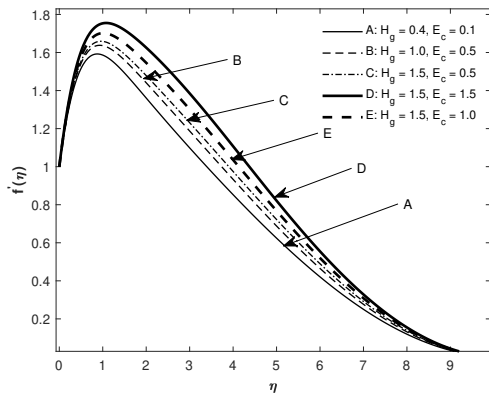


Figure 4: Velocity variation for varying values of  $H_g$  and  $E_c$  with  $W_p = 0.3$ ,  $E_{f_{pn}} = 0.01$ ,  $K_{rp} = 0.1$ ,  $M_p = 1$ ,  $\vartheta = 90$ ,  $\gamma = 0$ ,  $G_t = 5$ ,  $G_m = 1$ ,  $L_e = 0.3$ ,  $N_t = N_b = 0.1$ .

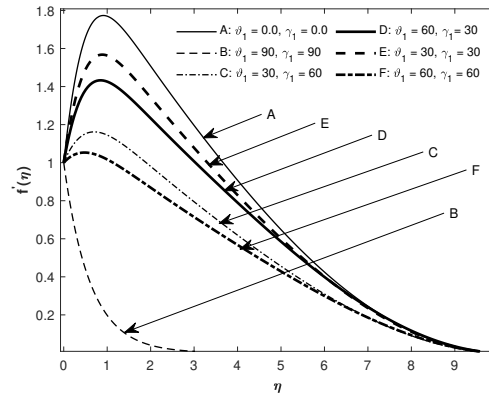


Figure 7: Velocity variation for a combination of the inclination angles  $\vartheta_1$  and  $\gamma_1$  with  $E_{f_{pn}} = 0.01$ ,  $W_p = 0.3$ ,  $K_{rp} = 0.1$ ,  $M_p = 1$ ,  $H_g = 0.4$ ,  $G_t = 5$ ,  $G_m = 1$ ,  $L_e = 0.3$ ,  $N_t = N_b = 0.1$ .

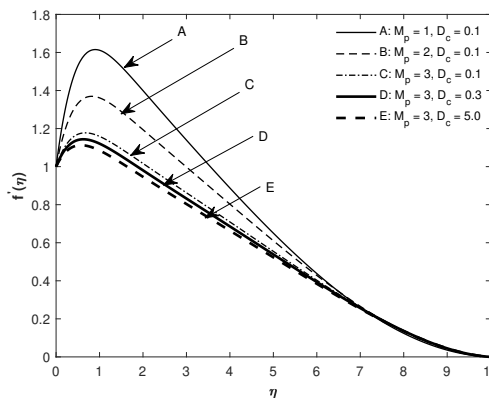


Figure 5: Velocity variation for varying values of  $M_p$  and  $D_c$  with  $W_p = 0.3$ ,  $K_{rp} = 0.1$ ,  $H_g = 0.4$ ,  $\vartheta = 90$ ,  $\gamma = 0$ ,  $L_e = 0.3$ ,  $G_t = 5$ ,  $G_m = 1$ ,  $N_t = N_b = 0.1$ .

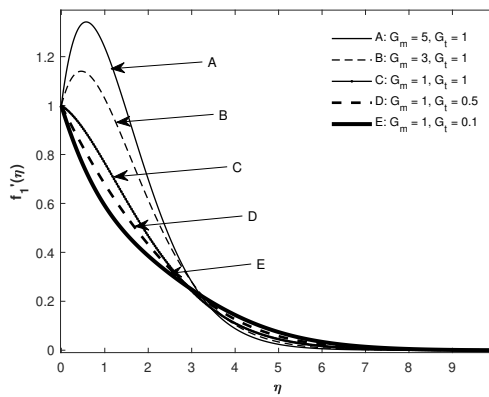


Figure 8: Velocity variation for varying values of  $G_t$  and  $G_m$  with  $E_{f_{pn}} = 0.7$ ,  $W_p = 0.1$ ,  $K_{rp} = 0.1$ ,  $M_p = 1$ ,  $H_g = 0.4$ ,  $G_t = 5$ ,  $G_m = 1$ ,  $E_c = 0.5$ ,  $L_e = 0.3$ ,  $N_t = N_b = 0.1$ .

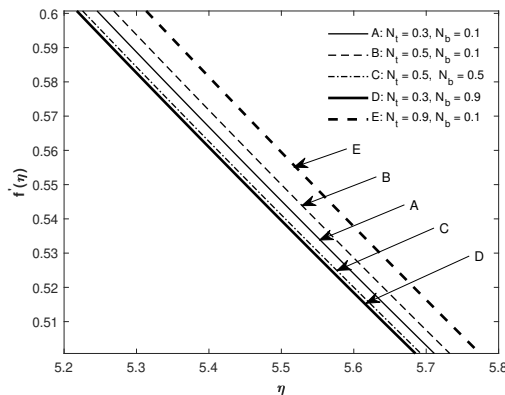


Figure 6: Velocity for varying values of  $N_t$  and  $N_b$  with  $W_p = 0.3$ ,  $K_{rp} = 0.1$ ,  $M_p = 1$ ,  $H_g = 0.4$ ,  $\vartheta = 90$ ,  $\gamma = 0$ ,  $G_t = 5$ ,  $G_m = 1$ ,  $N_t = N_b = 0.1$ ,  $L_e = 0.3$ .

that is,  $\vartheta_1 = \gamma_1 = 0$ . Moreover, for any given pair of inclination angles,  $\vartheta_1$  and  $\gamma_1$  the velocity profile is larger whenever  $\vartheta_1 > \gamma_1$ . Similar effects are noticed on the temperature profile in free stream ( $\eta > 5$ ). Figures 14 and 23 clearly show that the inclination angles have an entirely opposite effect on the temperature profile closer to the wall and concentration profile. The magnitude of the temperature and concentration profiles achieve their maximum value when inclination angles are largest, that is,  $\vartheta_1 = \gamma_1 = 90$ . For any pair of the inclination angles  $\vartheta_1$  and  $\gamma_1$  the profile is larger when  $\gamma_1 > \vartheta_1$ .

The impact of the Williamson factor on the velocity profile, tem-

perature profile and concentration profile is depicted in the Figures 2, 15 and 25. It is revealed that increasing the Williamson parameter retards the fluid velocity and fluid temperature, whereas the nanoparticles concentration is enhanced. Figures 5, 12 and 19 depict the impact of  $M_p$  on the velocity, temperature and concentration profiles, respectively. It is clear that the larger value of  $M_p$  suppresses the velocity profile and magnifies the temperature and concentration profiles. The presence of the magnetic field induces a retarding force called Lorentz force which suppresses fluid flow and consequently raises fluid temperature and nanoparticle concentration.

Figures 4 and 22 display the velocity profiles and concentration profiles of the fluid flow for different values of the Eckert number  $E_c$ . It is observed that upgrading the Eckert number grows the velocity of the fluid and reduces the concentration of the nanoparticles within the fluid. The influence of the effective prandtl number  $E_{f_{pn}}$  on the velocity distribution, temperature distribution and nanoparticle fraction is depicted in Figures 3, 13, 20 and 21. It is noticed that, the effect of increasing the effective Prandtl number is to suppress the concentration profile near the wall, the velocity profile and the temperature profile. Further away from the wall ( $\eta > 2$ ), enlarged effective Prandtl number enhances the concentration profile. The enlargement of the effective Prandtl number generates opposing force against the fluid flow resulting in a reduced fluid velocity and fluid temperature and consequently reduced momentum and thermal boundary layer.

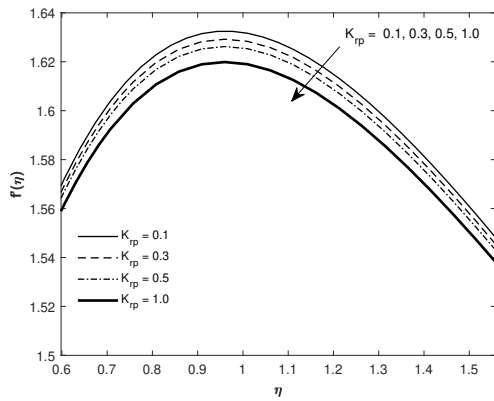


Figure 9: Velocity variation for varying values of  $K_{rp}$  with  $E_{fpm} = 0.7$ ,  $W_p = 0.1$ ,  $K_{rp} = 0.1$ ,  $M_p = 1$ ,  $H_g = 0.4$ ,  $G_t = 5$ ,  $G_m = 1$ ,  $E_c = 0.5$ ,  $L_e = 0.3$ ,  $N_t = N_b = 0.5$ ,  $\vartheta = 90$ ,  $\gamma = 0$ .

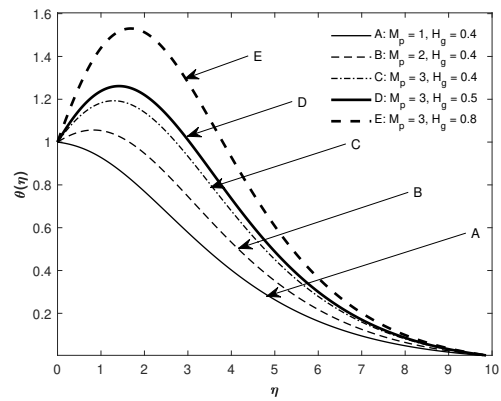


Figure 12: Temperature variation with varying values of  $M_p$  and  $H_g$  with  $G_t = 10$ ,  $G_m = 1$ ,  $D_c = 0.5$ ,  $E_c = 0.5$ ,  $\vartheta_1 = 90$ ,  $\gamma_1 = 0$ ,  $L_e = 0.3$ .

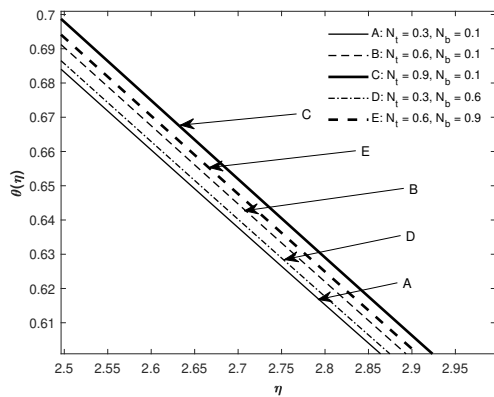


Figure 10: Temperature variation for  $N_t$  and  $N_b$  with  $\vartheta_1 = 90$ ,  $\gamma_1 = 0$ ,  $E_{fpm} = 0.01$ ,  $W_p = 0.3$ ,  $K_{rp} = 0.1$ ,  $M_p = 1$ ,  $H_g = 0.4$ ,  $G_t = 5$ ,  $G_m = 1$ ,  $L_e = 0.3$ .

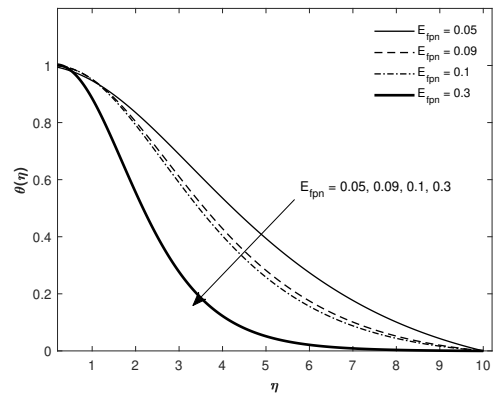


Figure 13: Temperature variation for varying various values of  $E_{fpm}$  with  $M_p = 1$ ,  $G_t = 10$ ,  $G_m = 1$ ,  $D_c = 0.5$ ,  $E_c = 0.5$ ,  $\vartheta_1 = 90$ ,  $\gamma_1 = 0$ ,  $L_e = 0.3$ .

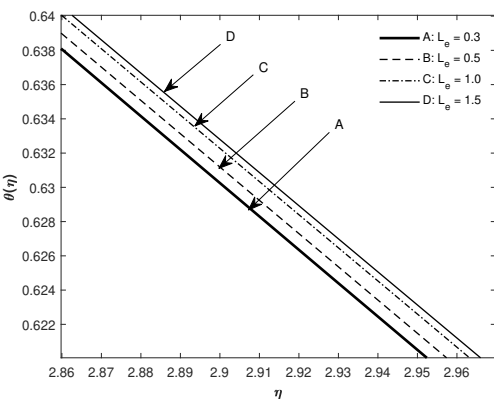


Figure 11: Temperature variation with varying values of  $L_e$  with  $E_{fpm} = 0.09$ ,  $M_p = 1$ ,  $G_t = 10$ ,  $G_m = 1$ ,  $D_c = 0.5$ ,  $E_c = 0.5$ ,  $\vartheta_1 = 90$ ,  $\gamma_1 = 0$ .

Figures 11 and 24 disclose the impact of the Lewis number  $L_e$  on the temperature and concentration profiles, respectively. An escalation of the Lewis number declines the concentration profile and enhances the temperature profile. It is clear that the thermal boundary layer is magnified whereas, the concentration boundary layer viscosity is lowered.

The influence of both the thermophoresis parameter  $N_t$  and the Brownian motion parameter  $N_b$  on the velocity profile, temperature profile and concentration profile are depicted in Figures 6, 10 and

18, respectively. Enlarged values of the thermophoresis parameter magnify the velocity profile, temperature profile and the nanoparticles concentration. The rise in the thermophoresis parameter tends to raise the fluid temperature due to increased temperature gradient across the thermal boundary layer.

Increasing the magnitude of the Brownian motion parameter  $N_b$  has the effect of suppressing the fluid velocity and nanoparticle concentration, whereas the fluid temperature is raised. The small random fluctuations of the nanoparticles in the fluid heats up the boundary layer, consequently raising the temperature of the fluid.

The role of  $G_m$  and  $G_t$  on the velocity, temperature and concentration profiles are depicted in Figures 8, 17 and 27. It is revealed that the fluid velocity is boosted with enlarged values of  $G_t$  and  $G_m$ . On the contrary, the fluid temperature and fluid concentration declines with escalating values of  $G_t$  and  $G_m$ .

Figures 16 and 26 display the impact of the chemical reaction parameter  $K_{rp}$  on the temperature and concentration of the fluid. Escalating values of the chemical reaction parameter magnifies the fluid temperature and diminishes the fluid concentration. Figure 16 also portrays the effect of the parameter  $N_{tb}$  on the temperature profile. It is observed that raising the value of  $N_{tb}$  enhances the fluid temperature.

The influence of the heat generation parameter  $H_g$  on the velocity, temperature and concentration profiles are shown in Figures 4, 12 and 19. It is distinctly shown that escalating values of  $H_g$  upgrades the velocity and temperature profiles and declines the concentration

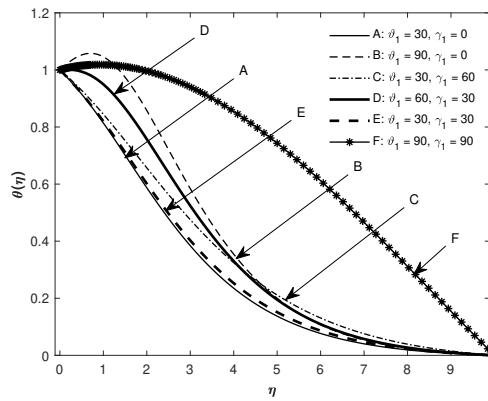


Figure 14: Temperature variation for varying values of the inclination angles  $\vartheta_1$  and  $\gamma_1$  with  $M_p = 1$ ,  $G_t = 10$ ,  $G_m = 1$ ,  $D_c = 0.5$ ,  $E_c = 0.5$ ,  $\vartheta_1 = 90$ ,  $\gamma_1 = 0$ ,  $L_e = 0.3$ .

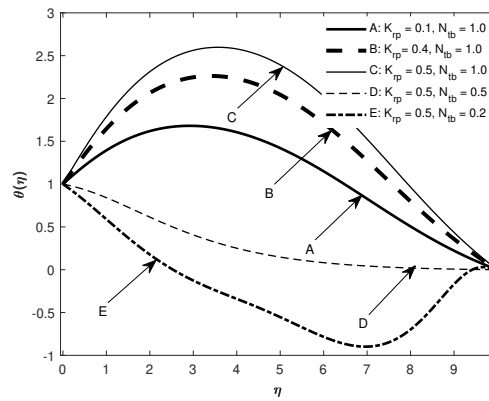


Figure 16: Temperature variation for varying values of  $K_{rp}$  and  $N_{tb}$  with  $M_p = 1$ ,  $G_t = 1$ ,  $G_m = 5$ ,  $E_c = 0.5$ ,  $\vartheta_1 = 30$ ,  $E_{f_{pn}} = 0.2$ ,  $\gamma_1 = 0$ ,  $L_e = 0.4$ .

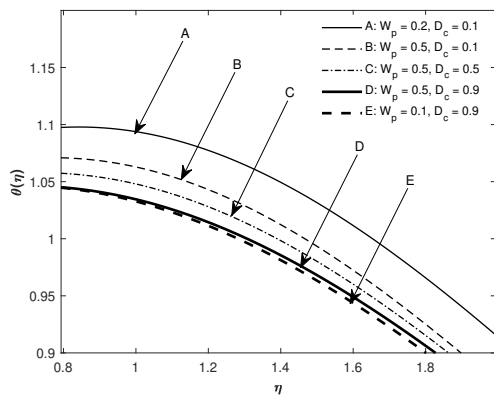


Figure 15: Temperature variation for varying values of  $W_p$  and  $D_c$  with  $M_p = 1$ ,  $G_t = 10$ ,  $G_m = 1$ ,  $E_c = 0.5$ ,  $\vartheta_1 = 90$ ,  $\gamma_1 = 0$ ,  $L_e = 0.3$ .

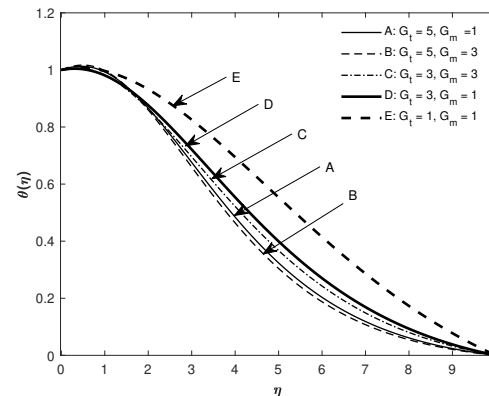


Figure 17: Temperature variation for varying values of  $G_t$  and  $G_m$  with  $W_p = 0.1$ ,  $H_g = 0.5$ ,  $K_{rp} = 0.1$ ,  $M_p = 1$ ,  $G_t = 1$ ,  $G_m = 5$ ,  $E_c = 0.5$ ,  $\vartheta_1 = 90$ ,  $E_{f_{pn}} = 0.09$ ,  $\gamma_1 = 0$ ,  $L_e = 0.3$ .

profile.

The influence of the Darcy number  $D_c$  on the velocity, temperature and nanoparticle concentration is portrayed in Figures 5, 15 and 22, respectively. It is observed that the velocity and temperature fields decline with an increment of the Darcy number. On the other hand, the nanoparticle concentration goes up with increased value of the Darcy number. The growing value of the Darcy number means that the resistance offered by the porous medium to the fluid movement also rises, hence the deterioration in the profiles of the temperature and velocity fields,

Table II: Values of  $C_f Re^{1/2}$ ,  $-\theta'(0)$  and  $\phi'(0)$  for varying values of  $E_{f_{pn}}$ ,  $\vartheta_1$ ,  $\gamma_1$ , and  $H_g$  taking  $W_p = K_{rp} = D_c = L_e = N_b = N_t = 0.1$ ,  $G_m = M_p = 1$ ,  $G_t = 5$  and  $E_c = 0.5$

$E_{f_{pn}}$	$\vartheta_1$	$\gamma_1$	$H_g$	$C_f Re^{1/2}$	$-\theta'(0)$	$-\phi'(0)$
0.2	0	90	0.1	-1.0280	0.12550	0.39887
0.5				-1.0280	0.2250	0.317804
0.7				-1.0280	0.30617	0.25338
	30			-1.1368	0.23708	0.29770
	45			-1.2354	0.17584	0.33948
		45		0.7924	0.41963	0.24827
		30		1.2727	0.35870	0.48531
			0.3	1.2205	0.32679	0.41665
			0.4	1.2992	0.25685	0.37536

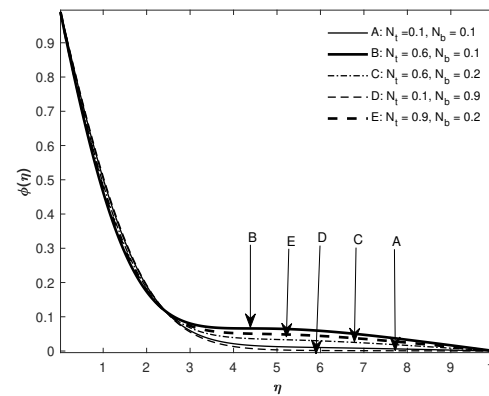


Figure 18: Concentration variation for varying values of  $N_t$  and  $N_b$  with  $W_p = 0.1$ ,  $G_t = 10$ ,  $G_m = 1$ ,  $E_c = 0.5$ ,  $\vartheta_1 = 90$ ,  $\gamma_1 = 0$ ,  $L_e = 0.3$ .

Tables II - V depict the influence of various parameters on the skin friction coefficient, Nusselt number and Sherwood number. It is revealed that the value of the skin friction coefficient is magnified with parameters rise in the values of the parameters  $H_g$ ,  $W_p$ ,  $K_{rp}$ ,  $L_e$  and  $N_b$ . On the contrary, the values of the skin friction coefficient decline with rising values of the parameters  $\vartheta_1$ ,  $D_c$  and  $N_t$ . We also deduce from the tables that the magnitude of the Nusselt number rises with larger values of the parameters  $\gamma_1$ ,  $E_{f_{pn}}$ ,  $W_p$ ,  $N_{tb}$  and  $D_c$ . Conversely, the Nusselt number value declines with escalating values of the parameters  $\vartheta_1$ ,  $H_g$ ,  $K_{rp}$ ,  $L_e$ ,  $N_t$  and  $N_b$ . Furthermore,

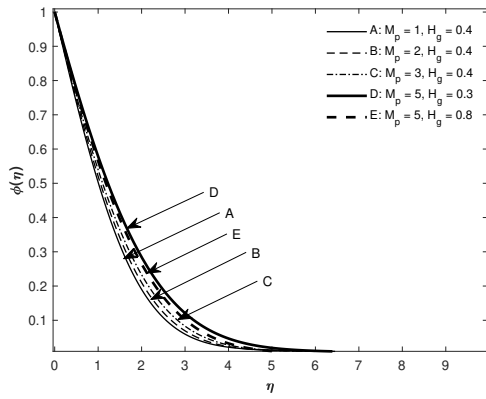


Figure 19: Concentration variation for varying values of  $M_p$  and  $H_g$  with  $W_p = 0.1$ ,  $G_t = 10$ ,  $G_m = 1$ ,  $E_c = 0.5$ ,  $\vartheta_1 = 90$ ,  $\gamma_1 = 0$ ,  $L_e = 0.3$ .

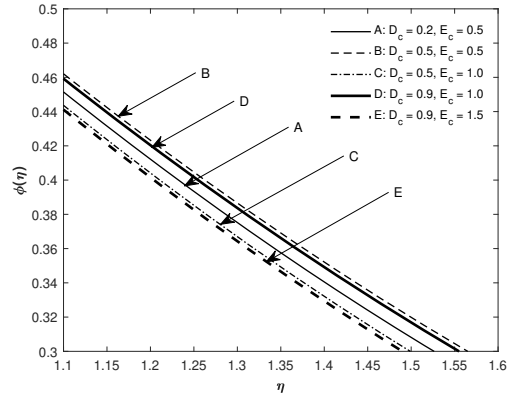


Figure 22: Concentration variation for varying values of  $D_c$  and  $E_c$  with  $G_t = 10$ ,  $G_m = 1$ ,  $\vartheta_1 = 90$ ,  $\gamma_1 = 0$ ,  $L_e = 0.3$ .

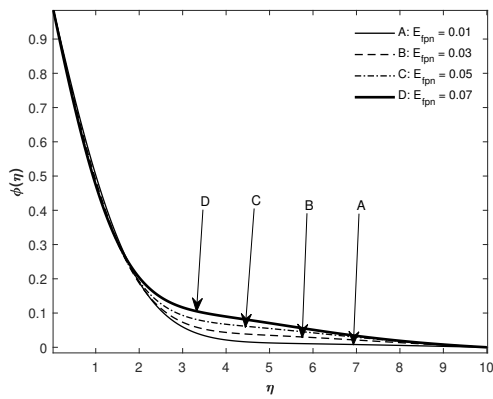


Figure 20: Concentration variation for varying values of  $E_{f_{pn}}$  with  $G_t = 10$ ,  $G_m = 1$ ,  $E_c = 0.5$ ,  $\vartheta_1 = 90$ ,  $\gamma_1 = 0$ ,  $L_e = 0.3$ .

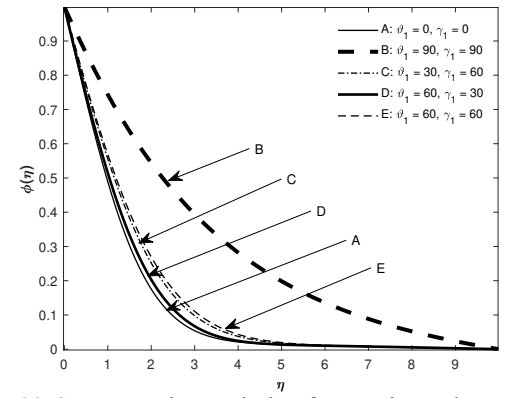


Figure 23: Concentration variation for varying values of  $\vartheta_1$  and  $\gamma_1$  with  $G_t = 10$ ,  $G_m = 1$ ,  $E_{f_{pn}} = 0.09$ ,  $\gamma_1 = 0$ ,  $L_e = 0.3$ .

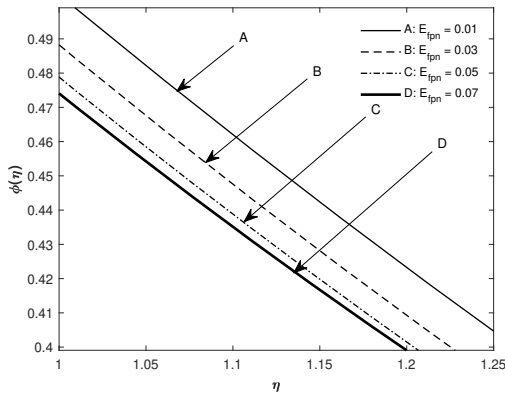


Figure 21: Concentration variation close to the wall for varying values of  $E_{f_{pn}}$  with  $G_t = 10$ ,  $G_m = 1$ ,  $E_c = 0.5$ ,  $\vartheta_1 = 90$ ,  $\gamma_1 = 0$ ,  $L_e = 0.3$ .

Table III: Values of  $C_f Re^{1/2}$ ,  $-\theta'(0)$  and  $\phi'(0)$  for varying values of  $W_p$ ,  $D_c$ ,  $K_{rp}$  and  $L_e$  taking  $E_{f_{pn}} = 0.7$ ,  $\vartheta_1 = 45$ ,  $\gamma_1 = 30$ ,  $H_g = 0.4$ ,  $N_b = N_t = 0.1$ ,  $G_m = M_p = 1$ ,  $G_t = 5$  and  $E_c = 0.5$

$W_p$	$D_c$	$K_{rp}$	$L_e$	$C_f Re^{1/2}$	$-\theta'(0)$	$-\phi'(0)$
0.1	0.1	0.1	0.5	1.2992	0.2569	0.3754
0.11				1.1575	0.4872	-0.2427
0.12				1.2518	2.4655	-4.7347
	0.2			0.8220	1.0090	-2.0612
	0.3			0.5878	1.2186	-2.305
		0.4		0.6345	0.6519	-0.3067
		0.5		1.1036	0.2890	0.5871
			1	0.7956	0.4847	0.7622
			2	1.1345	0.1236	1.7032

Table IV: Values of  $C_f Re^{1/2}$ ,  $-\theta'(0)$  and  $\phi'(0)$  for varying values of  $N_t$ ,  $N_b$ ,  $M_p$  and  $E_c$  taking  $W_p = K_{rp} = 0.1$ ,  $\vartheta_1 = 0$ ,  $\gamma_1 = 90$ ,  $H_g = 0.4$ ,  $G_m = 1$ ,  $G_t = 5$ ,  $D_c = 0.1$ ,  $E_{f_{pn}} = 0.7$  and  $L_e = 0.5$

$N_t$	$N_b$	$M_p$	$E_c$	$C_f Re^{1/2}$	$-\theta'(0)$	$-\phi'(0)$
0.1	0.1	1	0.1	-1.0280	0.3527	0.2320
0.5	0.1	1	0.1	-1.2409	0.3407	-0.4751
0.5	0.5	1	0.1	-1.0280	0.2926	0.2854
0.5	0.5	5	0.1	-1.0280	0.2926	0.2854
0.5	0.5	5	0.5	-1.0280	0.2926	0.2854

we deduce that the magnitude of the Sherwood numbers upgrade for greater values of the parameters  $\vartheta_1$ ,  $K_{rp}$ ,  $L_e$  and  $N_b$  and are suppressed for larger values of  $\gamma_1$ ,  $H_g$ ,  $E_{f_{pn}}$ ,  $W_p$ ,  $D_c$ ,  $N_{tb}$  and  $N_t$ . Table IV show that  $M_p$  and  $E_c$  have no effect on the magnitude of the skin friction coefficient, Nusselt number and Sherwood number provided  $N_t = N_b$ , that is,  $N_{tb} = 1$ . Finally, Table V shows that the variation of the parameters  $G_t$  and  $G_m$  have no effect on the skin friction, Nusselt number and Sherwood number. It is also shown that larger values of the parameter  $N_{tb}$  raises the Nusselt number, diminishes the Sherwood number and have no effect on the skin friction coefficient.

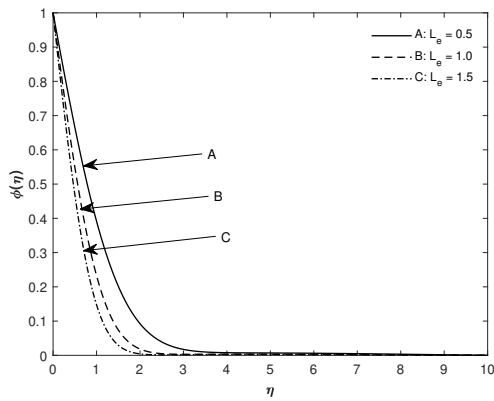


Figure 24: Concentration variation for varying values of  $L_e$  and  $\gamma_1$  with  $G_t = 10$ ,  $G_m = 1$ ,  $E_{f_{pn}} = 0.09$ ,  $\gamma_1 = 0$ .

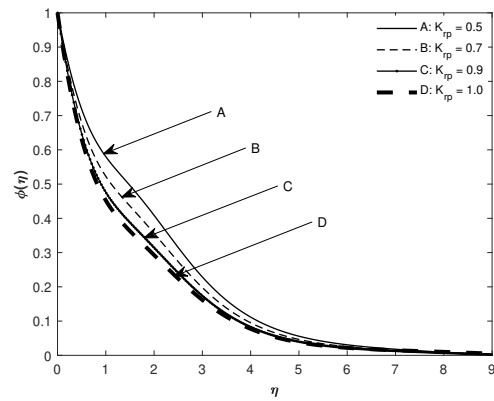


Figure 26: Concentration variation for varying values of  $K_{rp}$  with  $G_t = 1$ ,  $G_m = 5$ ,  $E_{f_{pn}} = 0.7$ ,  $\vartheta_1 = 30$ ,  $\gamma_1 = 30$ .

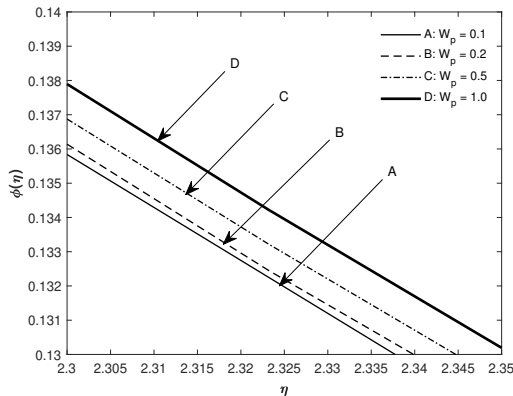


Figure 25: Concentration variation for varying values of  $W_p$  with  $G_t = 10$ ,  $G_m = 1$ ,  $E_{f_{pn}} = 0.09$ ,  $\gamma_1 = 0$ ,  $L_e = 0.3$ .

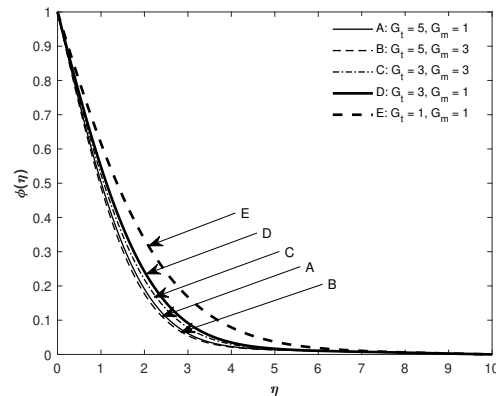


Figure 27: Concentration variation for varying values of  $G_t$  and  $G_m$  with  $W_p = 0.1$ ,  $K_{rp} = 0.1$ ,  $E_c = 0.5$ ,  $H_g = 0.5$ ,  $M_p = 1$ ,  $E_{f_{pn}} = 0.09$ ,  $\vartheta_1 = 90$ ,  $\gamma_1 = 0$ ,  $L_e = 0.3$ .

Table V: Values of  $C_f Re^{1/2}$ ,  $-\theta'(0)$  and  $\phi'(0)$ , for varying values of  $N_{tb}$ ,  $G_t$  and  $G_m$  taking  $W_p = K_{rp} = 0.1$ ,  $\vartheta_1 = 0$ ,  $\gamma_1 = 90$ ,  $H_g = 0.4$ ,  $G_m = 1$ ,  $G_t = 5$ ,  $D_c = 0.1$ ,  $E_{f_{pn}} = 0.7$  and  $L_e = 0.5$

$N_{tb}$	$G_t$	$G_m$	$C_f Re^{1/2}$	$-\theta'(0)$	$-\phi'(0)$
1	5	1	-1.0280	0.3527	0.2320
0.5			-1.0280	0.33861	-0.33364
0.1			-1.0280	0.23625	0.41390
	3		-1.0280	0.23625	0.41390
	1		-1.0280	0.23625	0.41390
		0.5	-1.0280	0.23625	0.41390
		0.1	-1.0280	0.23625	0.41390

V. CONCLUSION

In the current study, we have investigated the impact of inclined channel, effective Prandtl number, Brownian motion parameter, variable magnetic field and thermophoresis on MHD Williamson nanofluid. Numerical solutions are obtained using MATLAB bvp4c package. Significant outcomes of investigations are listed below:

1. The magnitude of the velocity profile is enhanced with increasing values of the parameters  $H_g$ ,  $E_c$ ,  $G_t$ ,  $G_m$ ,  $K_{rp}$ ,  $N_{tb}$  and  $N_t$  and declines with enlarged values of the parameters  $W_p$ ,  $E_{f_{pn}}$ ,  $M_p$ ,  $D_c$ ,  $N_b$ ,  $K_{rp}$ ,  $\vartheta_1$  and  $\gamma_1$ .
2. The temperature profile grows with larger values of the parameters  $L_e$ ,  $M_p$ ,  $H_g$ ,  $\vartheta_1$ ,  $\gamma_1$ ,  $N_t$  and  $N_b$  and falls with escalating values of the parameters  $E_{f_{pn}}$ ,  $W_p$ ,  $G_t$ ,  $G_m$  and  $D_c$ .

3. Magnified values of the parameters  $N_t$ ,  $M_p$ ,  $D_c$ ,  $W_p$ ,  $\vartheta_1$ ,  $\gamma_1$  and  $E_{f_{pn}}$  cause an increase in the nano-particle concentration. Inverse effect on the nano-particles concentration is noticed for larger values of the parameters  $D_c$ ,  $W_p$ ,  $K_{rp}$ ,  $G_m$ ,  $G_t$  and  $E_{f_{pn}}$ .
4. The velocity distribution is largest when both  $\vartheta_1$  and  $\gamma_1$  attain their lowest values. Also, for any given pair of  $\vartheta_1$  and  $\gamma_1$  values the velocity profile is larger whenever  $\vartheta > \gamma_1$ . The parameters  $\vartheta_1$  and  $\gamma_1$  have an opposite effect on the temperature and concentration profiles.
5. The magnitude of the skin friction is raised with increasing values of  $\gamma_1$ ,  $W_p$ ,  $D_c$  and  $E_{f_{pn}}$  is lowered for larger values of  $H_g$ ,  $L_e$ ,  $K_{rp}$ ,  $N_t$ ,  $N_b$  and  $\vartheta_1$ .
6. The magnitude of the Nusselt number increases with increasing values of  $W_p$ ,  $D_c$ ,  $\gamma_1$  and  $E_{f_{pn}}$  and declines for escalating values of the parameters  $K_{rp}$ ,  $H_g$ ,  $L_e$ ,  $N_t$ ,  $N_b$  and  $\vartheta_1$ .
7. Rising values of the parameters  $K_{rp}$ ,  $L_e$ ,  $N_b$  and  $\vartheta_1$  causes an increase in the magnitude of the Sherwood number. Inversely, the magnitude of the Sherwood number falls with rising values of  $D_c$ ,  $W_p$ ,  $H_g$ ,  $N_t$ ,  $\gamma_1$  and  $E_{f_{pn}}$ .
8. There is no change in the magnitude of the skin friction coefficient, Nusselt number and Sherwood number when the values of the parameter  $E_c$  and  $M_p$  are varied provided  $N_t = N_b$ .

Most of the findings listed above are not entirely new but are also found in previous literature. Results which stands out in the current study are that the enlargement of the effective Prandtl number suppresses the velocity profile, temperature profile and concentration

profile closer to the wall ( $\eta < 2$ ). In addition, magnification of both the inclination angles  $\vartheta_1$  and  $\gamma_1$  downturn the velocity profile and the profile is largest when  $\vartheta_1$  and  $\gamma_1$  are lowest, i.e. when  $\vartheta_1 = \gamma_1 = 0$ . Reversed behaviour was witnessed for the temperature and concentration profiles. Finally, the variation of the Eckert number and magnetic parameter have no effect on the skin friction, Nusselt number and Sherwood number when  $N_{tb} = 1$ .

REFERENCES

[1] M. S. Alam, M. M. Rahman, and A. Satter, "Transient magneto-hydrodynamic free convective heat and mass transfer flow with thermophoresis past a radiate inclined permeable plate in the presence of variable chemical reaction and temperature dependent viscosity", *Nonlinear Analysis: Modelling and Control*, vol. 14, no. 1, pp. 3-20, 2009.

[2] S. Bilal, K. U. Rehman, M. Y. Malik, A. Hussain, and M. Khan, "Effects of temperature dependent conductivity and absorption /generative heat transfer on MHD 3 dimensional flow of Williamson fluid due to bidirectional non-linear stretching surface", *Result Phys*, pp. 204- 212, 2017.

[3] J. Bouslimi, M. Omri, R. A. Mohamed, K. H. Mahmoud, S. M. Abo-Dahab, and M. S. Soliman, "MHD Williamson nanofluid flow over a stretching sheet through a porous medium under effects of joule heating, nonlinear thermal radiation, heat generation/absorption and chemical reaction", *Advances in Mathematical Physics*, vol. 2021, Article ID 9950993, 16 pages, 2021,

[4] G. Buzuzi, and A. N. Buzuzi, "Unsteady MHD convection flow and heat transfer past a vertical inclined plate in a porous medium with variable plate temperature with suction in a slip flow regime", *Int. J. of Appl. Math.*, vol. 32, no. 2, pp. 205-218, 2019.

[5] G. Buzuzi, "Inclined magnetic field and effective Prandtl number effects on unsteady MHD oscillatory flow past an inclined surface with constant suction and chemical reaction", *Journal of the Nigerian mathematical Society*", vol. 40, no. 3, pp. 227-244, 2021.

[6] S. U. S. Choi, "Enhancing thermal conductivity of fluids with nanoparticles", *Int. Mech. Eng. Cong. Exp. ASME., FED 231/MD*, vol. 66, pp. 99-105, 1995.

[7] H. D. Hunegnaw, "Unsteady boundary layer flow of Williamson nanofluids over a heated permeable stretching sheet embedded in a porous medium in the presence of viscous dissipation", *Journal of Naval Architecture and Marine Engineering*, doi.org/10.3329/jname.v18i1.51491, pp. 83-96, 2021.

[8] M. Khan, M. Y. Malik, T. Salahuddin, and A. Hussian, "Heat and mass transfer of Williamson nanofluid flow yield by an inclined Lorentz force over a nonlinear stretching sheet", *Results in Physics*, vol. 8, pp. 862-868, 2018.

[9] W. A. Khan, I. Pop, "Boundary layer flow of a nanofluid past a stretching sheet", *Int. J. Heat mass Transfer*, vol. 53, pp. 2477-2483, 2010.

[10] M. R. Krishnamurthy, B. C. Prasannakumara, B. J. Giresha, and R. S. R. Gorla, "Effect of chemical reaction on MHD boundary layer flow and melting heat transfer of Williamson nanofluid in porous medium", *Engineering Science and Technology, an International Journal*, vol. 19, pp. 53-61, 2016.

[11] T. P. Lyubimova, A. V. Perminov, and M. G. Kazimardanov, "Stability of quasi-equilibrium states and supercritical regimes of thermal vibrational convection of a Wiliamson fluid in zero gravity conditions", *International Journal of Heat and Mass Transfer*, vol. 129, pp. 406-414, 2019.

[12] S. Nadeem, and S. T. Hussian, "Flow fluid and heat transfer analysis of Williamson nanofluid", *Applied Nanosciences*, vol. 4, pp. 1005-1012, 2014.

[13] S. C. Reddy, K. Naikoti, and M. N. Rashidi, "MHD flow and heat transfer characteristics of Williamson nanofluid over a stretching sheet with variable thickness and variable thermal conductivity", *Transactions of A. Razmadze Mathematical Institute*, vol. 171, pp. 195-211, 2017.

[14] D. Gopal, N. Kishan, and C. S. K. Raju, "Viscous and Joule's dissipation on Casson fluid over a chemically reacting stretching sheet with inclined magnetic field and multiple slips", *Inf Med Unlocked*, vol. 9, pp. 154-160, 2017.

[15] D. Gurram, K. S. Balarugan, V. C. C. Raju, and N. Vedavathi, "Effect of chemical reaction on MHD Casson fluid flow past an inclined surface with radiation", *Skit Research Journal*, vol. 7, no. 1, pp. 53-59, 2017.

[16] S. Jain, and M. Kumari, "Inclined MHD Casson fluid flow over a permeable cylinder with viscous dissipation and chemical reaction", *International Journal of Mathematical Sciences*, vol. 17, pp. 205-226, 2018.

[17] C. P. Kumar, K. Raghunath, and M. Obulesu, "Thermal diffusion and inclined magnetic field effects on MHD free convection flow of Casson fluid past an inclined plate in conducting field", *Turkish Journal of Computer and Mathematics Education*, vol. 12, no. 13, 960-977, 2021.

[18] F. S. Ibrahim, A. M. Elaiw, and A. A. Bakr, "Effect of the chemical reaction and radiation absorption on the unsteady MHD free convection flow past a semi infinite vertical permeable moving plate with heat source and suction", *Commun. in Nonlin. Sci. and Numer. Simul.*, vol. 13, no. 6, pp. 1056-1066, 2008.

[19] E. Mgyari, "Comment on " Mixed convection boundary layer flow over a horizontal plate with thermal radiation" by A Ishak, *Heat mass Transfer*, DOI 10.1007/s00231-009-0552-3, vol. 46, pp. 509-810, 2010.

[20] E. Magyari, and A. Pantokratoras, "Note on the effect of thermal radiation in the linearized Roseland approximation on the heat transfer characteristics of various boundary layer flows", *International Communications in Heat and Mass Transfer*, vol. 38, pp. 554-556, 2011.

[21] S. Nadeem, and S. Akram, "Influence of inclined magnetic field on peristaltic flow of a Williamson fluid model in an inclined symmetric or asymmetric channel", *Mathematical Computer Modelling* , vol. 52, pp. 107-110, 2010.

[22] K. Rafique, and H. Alotaibi, "Numerical Simulation of Williamson nanofluid flow over an inclined surface: Kellar box analysis", *Applied Sciences*, https://doi.org/10.3390/app112311523, vol. 11, 2021.

[23] K. Rafique, M. I. M. Misiran, I. Khan, S. O. Alharbi, P. Thounthong, and K. S. Nisar, "Numerical solution of Casson nanofluid flow over a non-linear inclined surface with Soret and Dufour effects by Keller-method", *Frontier in Physics*, vol. 7, pp. 1-13, 2019.

[24] G. S. Reddy, S. K. Reddy, P. Durgaprasad, and S. V. Varma, "Diffusion-thermo and aligned magnetic field effects on force convection on flow past an inclined porous plate with first order chemical reaction", *IOSR Journal of Electrical and Electronics Engineering*, vol. 12, no. 3, pp. 25-33, 2017.

[25] P. Roja, T. S. Reddy, and N. B. Reddy, "Double diffusive convection-radiation interaction on unsteady Mhd flow of a micropolar fluid over a vertical moving porous plate embedded in a porous medium with heat generation and solet effects", *Int. J. of Engin. and Sci.*, vol. 1, no. 2, pp. 201-214, 2012.

- [26] N. Sandeep, and V. Sugunamma, "Radiation and inclined magnetic field effects on unsteady hydromagnetic free convection flow past an impulsively moving vertical plate in a porous medium", *J. Appl. Fluid. Mech.*, vol. 7, no. 2, pp. 275-286, 2014.
- [27] H. M. Shawky, N. T. M. Eldabe, K. A. Kamol, E. A. Abd-Aziz, "MHD flow with heat and mass transfer of Williamson nanofluid over stretching sheet through porous medium", *Microsyst Technol*, vol. 25, pp. 1155-1169, 2019.
- [28] K. Subbarayudu, S. Suneetha, and P. B. A. Reddy, "The assessment of time-dependent flow of Williamson fluid with radiative blood flow against a wedge, *Propulsion and Power Research*", vol. 9, no. 1, pp. 87-99, 2020.
- [29] R. V. Williamson, "The flow of pseudoplastic materials", *Industrial and Engineering Chemistry*, vol. 21, no. 11, pp. 1108-1111, 1929.
- [30] I. Wubset, and N. Mekonnen, "The investigation of MHD Williamson nanofluid over stretching cylinder with the effect of activation energy", *Advances in Mathematical Physics*, vol. article ID 9523630, 16 pages, 2020.
- [31] M. A. Seddeek, and M. S. Abdelmeguid, "Effects of radiation and thermal diffusivity on heat transfer over a stretching surface with variable heat flux", *Physics Letters A*, vol. 348, no. 36, pp. 172-179, 2006.
- [32] S. Shateyi, S. S. Motsa, and P. Sibanda, "The effects of Thermal Radiation, Hall currents, Soret, and Dufour on MHD Flow by Mixed Convection Over a Vertical Surface in Porous media", *Mathematical Problems in Engineering*, vol 2010, Article ID 627475, 20 pages, 2010.
- [33] C. Sivaraj, and M. A. Sheremet, "MHD natural convection in an inclined square porous cavity with a heat conducting solid block", *Journal of Magnetism and Magnetic Materials*, vol. 426, pp. 351-360, 2017.